

Hydrodynamic Design of Integrated Propulsor/Stern Concepts by Reynolds-Averaged Navier-Stokes Techniques

Rich Korpus^a, Bryan Hubbard^a, Paul Jones^a, Chel Stromgren^b, and James Bennett^c

^a Science Applications International Corporation, Ship Technology Division
134 Holiday Court, Suite 318, Annapolis, Maryland 21401 USA

^b Newport News Shipbuilding
Commercial Ship Eng., E56, Bldg. 600/1, Newport News, VA USA

^c Bath Iron Works Corporation
46 Church Road, Brunswick, Maine 04011 USA

A new tool has emerged to assist ship designers with the difficult task of propulsor/stern integration. Viscous flow computational methods, particularly Reynolds-Averaged Navier-Stokes (RANS) techniques, have left the realm of academics and entered practical service. When used in conjunction with traditional towing tank tests, the new capability has the potential to greatly improve the design process. This paper presents a number of practical examples to demonstrate this potential. The first demonstrates the effect of stern shape modifications on propeller inflow for a traditional single screw product carrier. The second utilizes RANS to investigate the efficiency of a podded propulsion system with tractor propeller for a high speed "wave piercer" hull form.

1. INTRODUCTION

Proper integration of hull and propulsor is essential for both the operating efficiency and vibratory behavior of a given design. Naval architects have traditionally utilized empirical techniques for this integration, and often use model testing to find the "effective wake" or "thrust deduction" needed by the propeller designer. Unfortunately, model tests require scaling assumptions, and only account for the presence of a propeller in very general ways.

Computational alternatives to model tests can circumvent these limitations by including the propeller's presence in simulations performed at full scale Reynolds numbers. Since propulsors are embedded in the hull boundary layer, however, any selected computational approach must rely at least on fully three-dimensional, Reynolds-Averaged Navier-Stokes (RANS) techniques.

While RANS techniques have traditionally remained limited to university or government research applications, recent improvements to their efficiency and reliability now allow them to meet the demands of ship design cycle time frames. This is not to say that RANS will replace the towing tank, but rather that the ship design process can benefit by the intelligent application of both. One advantage of

RANS is that less lead time is required than model tests, and a greater number of design alternatives can be investigated. RANS can also help guide the design process because both local flow and global measures of merit result from the solution.

Although RANS does reliably trend different design alternatives, it lacks sufficient fidelity for quantifying resistance of a final design. Tow tank testing is still required for this crucial step. An application where RANS can assist the tanks is for scaling of test results to full scale.

This paper is intended to serve two functions: 1) introduce the RANS system employed for hydrodynamic assessment at SAIC; and 2) demonstrate RANS on two practical applications. Development of the SAIC RANS system was initiated by more than ten years of Department of Defense support, and is heavily utilized for a number of submarine technology programs. It is unique, however, in that its later development has been driven mostly by industry, and has therefore become a practical design analysis tool. The applications presented are actual jobs performed for Newport News Shipbuilding and Bath Iron Works, and have been selected to demonstrate the utility of RANS for ship design.

2. APPROACH

The time-dependent viscous flow solutions presented in this study were obtained by solving the incompressible RANS equations in conjunction with a $k\varepsilon$ turbulence model. When non-dimensionalized by a characteristic length L , velocity V_0 , and density ρ , the Cartesian form of these governing equations can be written

$$\nabla \cdot \mathbf{V} = 0 \quad (1)$$

$$\frac{\partial \mathbf{V}}{\partial t} + \mathbf{V} \cdot \nabla \mathbf{V} + \nabla p - \frac{1}{\text{Re}} \nabla^2 \mathbf{V} - \nabla \cdot \boldsymbol{\tau} = \mathbf{F} \quad (2)$$

$$\frac{\partial k}{\partial t} + \mathbf{V} \cdot \nabla k - \left(\frac{1}{\text{Re}} + \nu_t \right) \nabla^2 k - P + \varepsilon = 0 \quad (3)$$

$$\begin{aligned} \frac{\partial \varepsilon}{\partial t} + \mathbf{V} \cdot \nabla \varepsilon - \left(\frac{1}{\text{Re}} + \frac{\nu_t}{1.3} \right) \nabla^2 \varepsilon - \frac{\varepsilon}{k} (c_{\varepsilon 1} P_{sol} + c_{\varepsilon 3} P_{irr}) \\ + c_{\varepsilon 2} \frac{\varepsilon^2}{k} = 0 \end{aligned} \quad (4)$$

where the Reynolds stress components τ_{ij} are defined by the Boussinesq approximation.

$$\tau_{ij} \equiv -\frac{2}{3} k \delta_{ij} + \nu_t S_{ij}, \quad S_{ij} = \frac{\partial u(i)}{\partial x^j} + \frac{\partial u(j)}{\partial x^i} \quad (5)$$

and $[x^1, x^2, x^3]^T$ represents the Cartesian position vector. \mathbf{V} represents the Cartesian velocity's vector $[u(1), u(2), u(3)]^T$, p the pressure, k the turbulent kinetic energy, and ε the turbulent dissipation rate. \mathbf{F} is an arbitrary body force used to represent propulsor effects. The quantity ν_t is defined as the linear eddy viscosity $.09 k^2/\varepsilon$, and Re the Reynolds number $L V_0/\nu$. The rate of production of k is represented by P , and production in the ε equation has been split into its solenoidal and irrotational components following Hanjalic and Launder (1980):

$$P = P_{sol} + P_{irr} \quad (6)$$

$$P_{sol} = 4[S_{12}^2 + S_{13}^2 + S_{23}^2] \quad (7)$$

$$P_{irr} = 2[S_{11}^2 + S_{22}^2 + S_{33}^2] \quad (8)$$

The modeling coefficients $C_{\varepsilon 1}$, $C_{\varepsilon 2}$, $C_{\varepsilon 3}$ are taken as constants set equal to (1.44, 1.92, 2.4), respectively.

The usual near-wall stiffness problem associated

with Eq.(4) has been circumvented herein by using the two-layer approach of Chen and Patel (1988,1989). The approach utilizes the $k\varepsilon$ model outlined above for most of the flow field, but a one-equation kl model in the viscous sublayer and buffer zone. Switching between ε and l dissipation models is performed automatically when the wall Reynolds number $\text{Re}_{wall} = \text{Re} \sqrt{k} \delta$ (δ being the nondimensional distance to the closest wall) becomes less than 300 (Chen and Korpus, 1993). Details of the l dissipation model can be found in Chen and Patel (1989) and will not be repeated here.

Computations about complex geometries requires that Equations (1) through (4) be first transformed into body fitted coordinates. This is accomplished by defining a curvilinear system (ξ^1, ξ^2, ξ^3) such that any physical boundary in the domain coincides with one or more surfaces of constant ξ^i . The system need not necessarily be orthogonal, and can be defined separately for each block of the grid. All independent variables in Equations (1) through (4) are then transformed to (ξ^1, ξ^2, ξ^3) space by chain rule while leaving the dependant variables Cartesian.

With the equations in their curvilinear form, the discretization is accomplished by linearizing each equation, over a computational element, then solving analytically by separation of variables. Evaluation of the analytic solution at the interior node of a computational element provides a stencil for the center point in terms of its nearest neighbors. Time derivatives are handled by the Euler implicit method, and unknowns from the previous time step are lumped into the source term. The resulting implicit system equations is solved by the alternating direction implicit (ADI) method in each cross-flow plane, and then swept repetitively in the streamwise direction. Detailed expressions for the coefficients of the finite-analytic stencil can be found in Chen et al. (1990).

Pressure coupling is supplied using a modified SIMPLER/PISO algorithm (Chen and Patel, 1989) that uses the strong conservation form of Eq. (1)

$$\frac{\partial \sqrt{g} U^1}{\partial \xi^1} + \frac{\partial \sqrt{g} U^2}{\partial \xi^2} + \frac{\partial \sqrt{g} U^3}{\partial \xi^3} = 0 \quad (9)$$

where U^i is the contravariant velocity $U(1) \partial \xi^1 / \partial x^1 +$

$U(2)\partial\xi^2/\partial x^1 + U(3)\partial\xi^3/\partial x^1$ and g is the determinant of the covariant fundamental metric tensor. The technique defines pseudo-velocities from the discretized form of Eq.(2) as:

$$U^i = \dot{U}^i + E^{ij} \frac{\partial p}{\partial \xi^j} \quad (10)$$

where \dot{U}^i and E^{ij} necessarily involve the finite-analytic coefficients, and will not be repeated here (see Chen and Korpus 1993).

A Poisson equation for pressure is then derived by substituting equation (10) into (9), and discretizing using central differences. By centering the differences in equation (10) on staggered grid locations, the resulting Poisson equation involves unknowns only at the grid nodes. The technique is thus unique in that it does not require staggered velocity and pressure variables.

To facilitate calculations around complex or moving geometries, the discrete forms from Eqs. (1) through (4) are embedded in a Chimera, multi-block environment. The solver works on one block at a time, and the only grid connectivity requirement is that the union of blocks spans the entire computational domain. Individual blocks are allowed to overlap arbitrarily, and inter-block communication is handled by conservative triquadratic interpolation. The overall approach has been extensively validated for both steady and unsteady three-dimensional applications (Korpus, 1995; Chen and Korpus, 1993; Weems and Korpus, 1994).

The advantages of Chimera grids are well demonstrated. Figure 1, which shows the tanker stern to be used as the first demonstration case. While the complete mesh is three-dimensional, the figure shows only these planes coincident with the hull surface, the water surface, and the hull centerplane. Note that each piece of the stern can be resolved to whatever level is locally required, and that blocks of extra resolution can be easily pieced in when needed (e.g. in way of the propeller)

It is this use of Chimera grids that has greatly increased the practicality of RANS. The fully 3D hull grid shown in Figure 1 can now be obtained in just a few days, as compared to conventional grids that could require many man-months.

Propelled simulations are performed by adding a non-zero body force vector \mathbf{F} in Equation (2) to represent propeller acceleration and swirl. Both propeller design studies and propeller analysis studies are possible. In the former a body force designed to represent the load distribution chosen by a designer is input into the RANS code, and the solution allowed to converge. The analysis case (i.e. where a propeller geometry is known, but not its load), is more complex. In that case, a vortex lattice propeller code is used to compute the body forces for an assumed inflow. The RANS code is then run using these forces for a small number of iterations. Since the body forces affect the inflow, the vortex lattice code must be re-run and the process iterated to convergence.

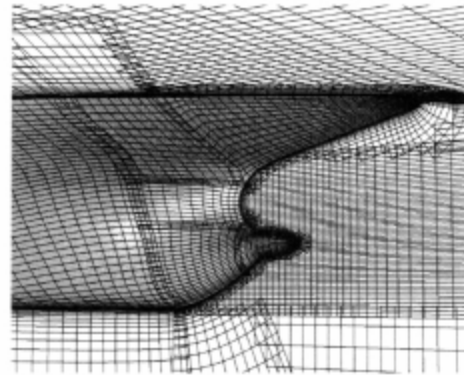


Figure 1: Chimera Grid Around Stern of Newport News Tanker

The entire described system, including Chimera grid scheme and propeller force method, has been integrated into an automated package to minimize user input. Coding is ANSI standard FORTRAN and C, and is vectorized for efficiency on large supercomputers. Simulations up to about 2.5 million grid points can be run on workstations while larger jobs typically run on CRAY supercomputers. Run times are in the order of 70 $\mu\text{sec}/\text{iteration}/\text{cell}$ on a 2 processor Silicone Graphics Inc. (SGI), OCTANE, and 14 $\mu\text{sec}/\text{iteration}/\text{cell}$ on a CRAY C90.

3. APPLICATIONS

Application of the described method will be demonstrated using calculations performed to support

actual ship design processes. The first example describes a comparison of two preliminary hull form candidates for Newport News Shipbuilding's "Double Eagle" product tanker hull form. The second describes an investigation of a podded propulsor option for Bath Iron Works' high speed "Wave-Piercer" hull form. Both examples focus on propeller/hull interaction simulations, and were chosen to demonstrate the utility of RANS for supporting practical design decisions.

3.1. Newport News Shipbuilding Hull Study

At one point during preliminary design of its "Double Eagle" product carrier, Newport News Shipbuilding (NNS) entertained a customer request to investigate low construction cost options to its existing stern design. One option called for maximizing the use of flat and rolled plate (as opposed to formed) in the stern. Calculation of life-cycle costs for such an option requires that the fuel efficiency of the "developable" stern be compared to the baseline design. Newport News decided to use RANS for quantifying these differences.

The two candidate stern forms are shown in Figure 2. The hull labeled NNS Model #333 represents the baseline case for comparison, whereas Model #334 represents the developable option.

Unpropelled calculations were made in each case to study the effect on nominal wake, and to support a rough propeller design for quantifying efficiency. Each hull was gridded using a similar mesh topology and about 450,000 points. Propelled

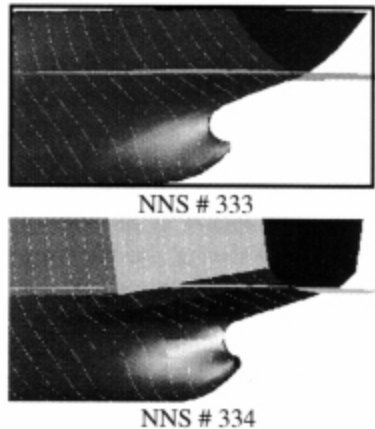


Figure 2: Comparison of Newport News Models # 333 and #334

calculations were also made for model #333 to compare with experiments. A grid of 1,300,000 points was used in that case because both sides of the boat are included, and because a high resolution patch (about 300,000 points) was added in way of the propeller (Figure 1). Grid generation using the Chimera scheme described above required about three weeks turn-around time.

All runs were started from uniform flow, and required approximately 2000 iterations to converge. Run times on an SGI Octane workstation are approximately 38 CPU hours for the unpropelled cases and 100 CPU hours for the propelled one. A model scale Reynolds number of 9.1 million was used to facilitate comparison to experiment, but full scale calculations can be performed at the cost of additional iterations. The propeller was loaded radially similar to B-screw series distribution, and chordwise using a sine distribution. The propeller's J , K_t , and K_q are 0.733, 0.1811, and 0.0237 respectively.

Sample post-processed results are given in Figures 3 through 6. Figure 3 shows near-surface streamlines similar to what would be seen in an experimental paint smear, and demonstrates that Model #334 exhibits greater separation than Model #333. Separation on the baseline hull is limited to very near the deadwood and under the bossing, but on the developable stern extends further forward and up.

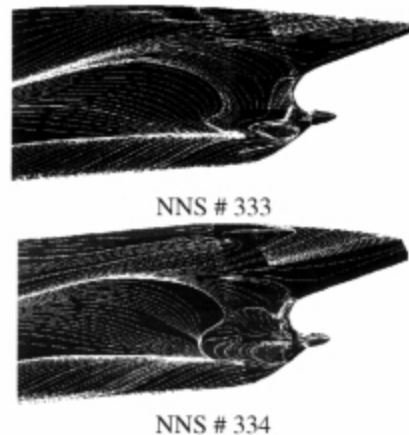
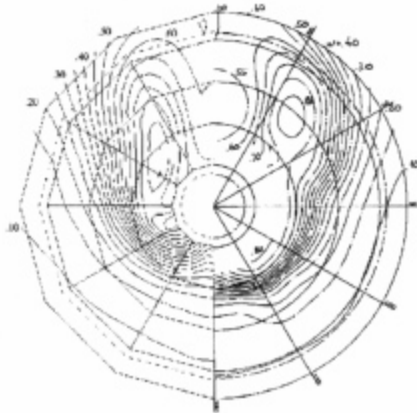


Figure 3: Streamlines for Newport News Model # 333 and # 334

The strong "streamline attraction" lines shown in each figure indicate the attachment point of the bilge vortices.

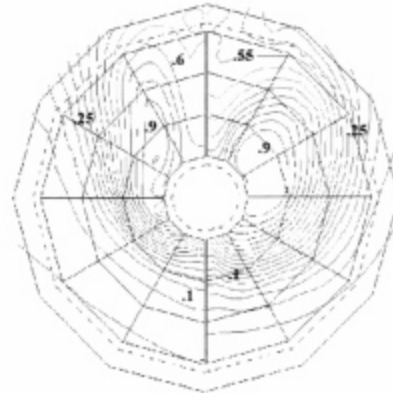
Figure 4 shows computed versus measured wake fractions in the plane of the propeller. Note that the measurements do not extend to the hull surface, but that the comparison is fairly good in the outer regions. The only significant difference seen is directly under the bossing where measurements show steeper gradients than calculations.



Calculation Experiment
Figure 4: Comparison of Computed and Experimental Propeller Plane Nominal Wakes.

A comparison of computed to measured forces shows that drag prediction is off by about 10%, but this is fairly typical for streamlined bodies with little drag. While RANS can reliably trend design alternatives, it can not yet compete with the towing tank for accurate final drag and powering numbers.

Figure 5 also shows wake fractions, but for a comparison between Model #333 and #334. It is immediately obvious that the differences are greater than those observed in Figure 4, and that Model #334 has a significantly greater wake. This result is also borne out by a comparison of computed drags which show Model #334's Cd to be 7% greater than Model #333's. The resulting increase in fuel bills over the life of the ship were computed to more than offset construction savings, and the customer was convinced not to pursue a developable stern option.



NNS # 333 NNS # 334

Figure 5: Comparison of Models # 333 and #334 Propeller Plane Nominal Wakes.

Figure 6 shows the streamwise velocities of a propelled Model # 333, at the propeller plane. When compared to the left sides of figures 4 and 5, the contours provide a graphic example of how propeller inflow cannot be derived from nominal wakes using simple extrapolation techniques. True effective wakes can be derived from RANS, however, by subtracting propeller potential flow velocities from the data shown in Figure 6. The resulting effect on propeller design will be substantial.

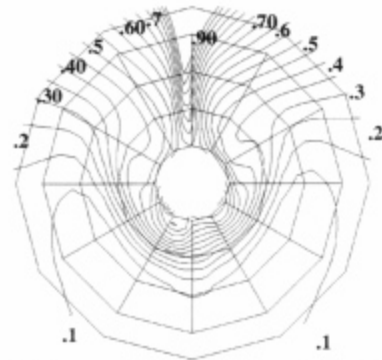


Figure 6: Streamwise Velocities of Model #333

3.2. Bath Iron Works Podded Propulsor Analysis

The "Wave-Piercer" hull forms now appearing hold great promise for both commercial and naval applications. Bath Iron Works Shipbuilding (BIW) plans to tap this potential, and has begun a program aimed at coupling Wave-Piercer hulls with advanced non-conventional propulsion systems. One option found worthy of detailed study is a twin installation of podded propulsors utilizing tractor propellers. The lack of historical experience to judge such new designs, however, has caused BIW to call on RANS for ranking the merits of such options. Particular concerns for the proposed pod combination include verifying the system's efficiency, and demonstrating that the prop wash will not stall the strut.

RANS simulations were therefore initiated for a commercially available motor pod geometry including strut, fillet, and lower stabilizer fin. The pods were aligned on an idealized hull surface, and yawed about their rotation axis to a two degrees bow out attitude. The inboard turning tractor propellers are represented by three-dimensional body forces, but only the starboard pod is included because of symmetry. Figure 7 shows the resulting geometry.

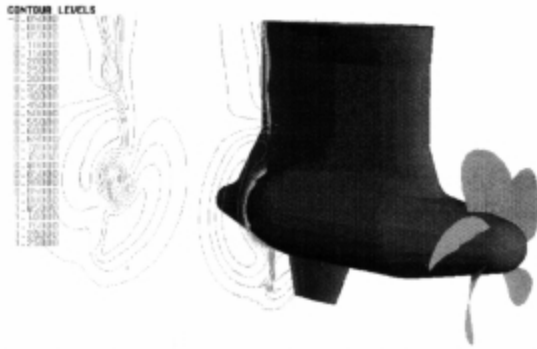


Figure 7: Contours of Axial Velocity for Podded Propulsor with Tractor Propeller.

The computational grid for this case required approximately 800,000 points, and about two weeks grid preparation time. A model scale Reynolds number of 0.9 million (based on pod length) was used to facilitate comparison to experiment. Convergence was achieved in about 60 CPU hours on an SGI Octane workstation, and additional

solutions (attitudes or speeds) with the same geometry can be generated in just a few days.

Sample results are shown in Figures 7 through 9. Figure 7 depicts contours of axial velocity in two planes perpendicular to the shaft axis. The first cut is taken just downstream of the stabilizer fin, and shows the fin tip vortex rolling up to starboard (i.e. the fin is lifting away from the ship centerplane).

Computed side force coefficients on the strut and fin (based on total wetted surface) are 0.0012 and 0.0069 respectively, with both being to starboard. This is indicative that the current pod attitude is not an optimal one. The main advantage of a tractor configuration is that the strut and fin can recapture rotational energy and convert it to thrust, thus improving total propulsive efficiency. This requires that both strut and fin lift in the direction of propeller rotation, and to approximately equal magnitudes. The current results indicate that the strut operates opposite to the propeller. Decreasing the pod yaw would change the strut lift back towards the centerline, and simultaneously decrease the fin's net lift to starboard. Fin redesign may be needed to achieve a side force balance between strut and pod.

Figure 8 shows off-body streamlines beginning upstream of the pod, and clearly demonstrates the propeller induced swirl.

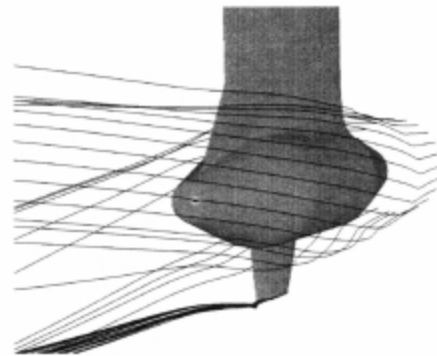


Figure 8: Off-Body and Stabilizer-Tip Streamlines for Podded Propulsor with Tractor Propeller.

The very strong fin tip vortex indicated confirms the side-force overloading of the fin mentioned above, and closer examination of the detailed surface flow reveals the fin to be partially stalled. Computed drag

indicates the fin contributes 14% to the total even though it comprises 7% of the wetted surface.

Although the design is not necessarily optimal with the current propeller, Figure 9 indicates that the system is recapturing some of the rotational energy in the propeller race.

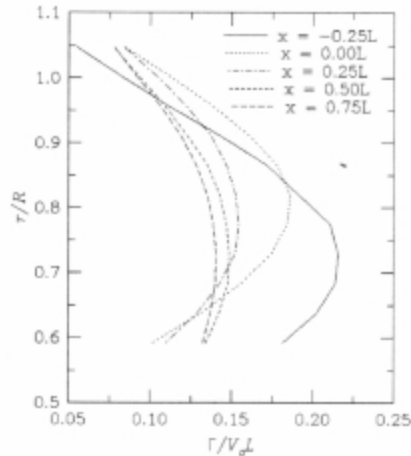


Figure 9: Circulation Behind Tractor Propeller

The figure shows distributions of total wake circulation (swirl) versus radius at five locations downstream of the propeller. The location labeled $x=-0.25$ is very near the propeller trailing edge, and indicates the total swirl induced in the flow. The curve labeled $x=0$ is at the pod yaw axis, and indicates that maximum circulation has already been reduced 20%. The remaining contours are all downstream of the strut, and indicate that approximately 40% of the propeller rotational energy has been recaptured.

4. CONCLUSIONS

Recent progress in RANS development has finally matured these complex methods into practical ship design assessment tools. Chimera gridding schemes combined with robust algorithms and turbulence models now enables complete propeller/hull flow simulations within practical design cycle turn-around times. When combined with the latest computers, RANS analyses for complete ship cases can be run on desktop

workstations thereby bringing total analysis costs in line with model tank tests.

RANS applications to the test cases described herein have demonstrated the potential for these tools to greatly improve the overall design process. The efficiency and vibration performance of single screw propellers, for example, could be increased through the a-priori knowledge of effective wake demonstrated in the Newport News example. Strut efficiency for podded propulsors (or any tractor combination) could likewise be improved using the knowledge of race swirl depicted by the second demonstration case.

As demonstrated, RANS may be effectively used in the design process to assess complex stern/hull flow. The RANS system provides the designer a fast, inexpensive assessment tool, which compliments towing tank tests and improves the overall design process. Furthering the interaction between the ship design community and RANS developers will help utilize this assessment tool to the best advantage of the ship industry.

REFERENCES

- Chen, H.C., and Korpus, R.A., 1993, "A Multi-Block Finite-Analytic Reynolds-Averaged Navier-Stokes method for 3-D Incompressible Flows," *ASME J. of Fluids Engineering*.
- Chen, H.C., and Patel, V.C., 1988, "Near-Wall Turbulence Models for Complex Flows Including Separation," *AIAA Journal*, Vol. 26, No. 4, pp. 641-648.
- Chen, H.C., and Patel, V.C., 1989, "The Flow Around Wing-Body Junctions," *Proceedings, 4th Symposium on Num. And Phys. Aspects of Aerodynamic Flows*, Long Beach, CA.
- Chen, H.C., Patel, V.C., and Ju, S., 1990, "Solutions of Reynolds-Averaged Navier-Stokes Equations for Three-Dimensional Incompressible Flows," *J. of Computational Physics*, Vol. 88, No.2, pp. 305-336.
- Hanjalic, K., and Launder, B.E., 1980, "Sensitizing the Dissipation Equation to Irrotational Strains," *ASME J. of Fluids Engineering*, Vol. 102.
- Korpus, R., 1995, "Six Years of Progress Under the ARPA SUBTECH Program," SAIC Report No. 95/1143.
- Korpus, R., and Falzarano, J.M., 1997, "Prediction of Viscous Ship Roll Damping by Unsteady Navier-Stokes Techniques," *J. of Offshore Mech. and Arctic Eng.*, vol. 119, no 2., pp. 108-113.
- Weems, K., and Korpus, R., et al., 1994, "Near-Field Flow Predictions for Ship Design," *Proceedings, 20th Symposium Naval Hydrodynamics*, Santa Barbara, CA.